A STUDY OF PROPELLER/WING INTERACTION INCLUDING THE EFFECT OF GROUND PROXIMITY

A P Harris* and D W Hurst**
Department of Aeronautics and Astronautics
University of Southampton
Southampton SO9 5NH
England

Abstract

Tests have been carried out on a propeller/nacelle/wing combination in the 3.5m x 2.6m low speed wind tunnel at the University of Southampton. Wing surface pressure distributions were measured both inside and outside of the propeller slipstream and also with the propeller blades removed. The wing was tested in a clean configuration and a high lift configuration with leading edge slat and single slotted trailing edge flap. In addition, the high lift configuration was tested at a ground clearance representative of full-scale aircraft in take-off or landing conditions. The propeller swirl caused an asymmetric loading on the clean wing. In the high lift configuration the leading edge slat significantly reduced this swirl effect over the wing. In ground effect an increase in lift occurred on the model. Approximately the same percentage increase was found to occur inside and outside of the propeller slipstream. Unsteady and time-averaged velocity measurements were acquired in the flowfield using a laser doppler anemometer. A low order panel method was used which gave satisfactory results for both the clean and high lift wing configurations with the propeller blades removed.

Nomenclature

b	half wing span, 1.143m
c	clean wing chord, 0.764m
c_b	blade chord [m]
C_L	spanwise lift coefficient [m^{-1}]
C_{Lo}	spanwise lift coefficient with propeller blades removed [m^{-1}]
C_p	pressure coefficient, $(P-P_\infty)/q_\infty$ [-]
C_P	power coefficient, $Q\omega/\rho n^3D^5$ [-]
C_T	thrust coefficient, $T/\rho n^2D^4$ [-]
d	longitudinal position relative to propeller disc [mm]
D	propeller diameter, 0.8m
h	distance from pivot point of the model to the ground [m]
J	advance ratio, V_∞/nD [-]
n	propeller rotational speed [revs.s^{-1}]
P	static pressure [N.m^{-2}]
P_∞	freestream static pressure [N.m^{-2}]
q_∞	freestream dynamic pressure, $0.5\rho V_\infty^2$ [N.m^{-2}]
Q	propeller torque [N.m]
r	radial distance along blade [m]
R	propeller radius, 0.4m
Re_b	blade Reynolds number, $\rho(V_\infty^2+\omega^2r^2)^{0.5}c_b/\mu$ [-]
Re_c	wing Reynolds number, $\rho V_\infty c/\mu$ [-]
T	propeller thrust [N]
U_{MEAN}	mean axial velocity [$m.s^{-1}$]
V_{MEAN}	mean swirl velocity [$m.s^{-1}$]
V_∞	freestream velocity [$m.s^{-1}$]
x	distance along chord from leading edge [m]
y	distance along span from centre line [m]
γ	ratio of spanwise lift coefficient to spanwise lift coefficient with propeller blades removed, C_L/C_{Lo} [-]
μ	air viscosity [$kg.m^{-1}.s^{-1}$]
ρ	air density [$kg.m^{-3}$]
ω	propeller angular velocity [$rads.s^{-1}$]

Introduction

An important aspect of propeller-powered aircraft design is the aerodynamic integration of the propeller and airframe. The propeller slipstream can affect the overall aerodynamic performance and stability of the aircraft. In a tractor configuration, the greatest interaction occurs between the propeller and the wing. The propeller induces both time-averaged and unsteady asymmetric aerodynamic loads on the wing [1-7]. The wing also has a reciprocal effect on the performance of the propeller [2,3]. This is partly due to an induced upwash which effectively alters the blade setting angle of each blade [8].

The interaction will be a maximum during take-off conditions when the propeller is highly loaded and high lift devices are deployed on the wing. The overall aerodynamic performance will be further complicated by the presence of the ground.

This paper presents the wind tunnel results for the interaction of a propeller and wing out of ground effect, with the wing in both a clean configuration and a high lift configuration with leading edge slat and single slotted trailing edge flap deployed. Results are also presented for the high lift wing at a height above the ground representative of full-scale aircraft in take-off or landing conditions. In this case, a moving ground facility was used to ensure that correct representation of the ground plane was produced.

---

* Graduate Research Assistant

** Wind Tunnel Facilities Manager

To obtain a full understanding of the characteristics of a wind tunnel model, it is essential to get detailed flow data throughout the entire flowfield. This information is also required during the development and validation of new theoretical codes. It is important that the data is obtained without causing flow interference by the insertion of probes and/or traverse systems into the working section. Tests were therefore undertaken using a Laser Doppler Anemometer (LDA) system to investigate the velocity distribution downstream of the propeller [9,10]. A theoretical and experimental comparison is also made between the results of a low order panel method and the wind tunnel results with the propeller blades removed.
The panel method is currently under development to include a steady state propeller model. Validation of the code will involve the comparison of surface pressure distributions on the wing and nacelle and also three dimensional velocity measurement comparisons in the flowfield using the LDA results.

Experimental Work

Wind Tunnel Facility

The tests were carried out in the 3.5m x 2.6m closed loop low speed wind tunnel at the University of Southampton. The tunnel had a maximum velocity of 50 m/s and was equipped with a moving ground facility of dimensions 5.5m x 2.4m situated in the floor of the working section.

LDA System

A diagram of the LDA set-up employed in these tests is shown in Figure 1. A 5 watt Ar-ion type laser was used and the measurements were carried out using a 3 dimensional Dantec system operating in back scatter mode. The focal length of the optics was 2000 mm which allowed the optical system to be mounted on a traverse system positioned outside of the wind tunnel test section. The beams passed through a large glass window installed in the wall of the working section. This ensured that the LDA system produced no interference to the airflow around the model. The seeding required by the LDA system was added to the airflow upstream of the working section contraction and introduced negligible interference to the freestream flow.
The doppler signal of each velocity component was processed by a Burst Spectrum Analyzer based on the Fourier transformation technique. Extensive data was given for each velocity component (e.g. mean velocity, rms velocity and turbulence levels).
The entire system, including traverse and Burst Spectrum Analyzers, was controlled by a micro computer for automatic operation.

Model Details

The wind tunnel model consisted of a propeller/nacelle/wing combination. This was mounted to a six component overhead force balance by two vertical support arms located at spanwise positions external to the propeller slipstream. The support arms were of adjustable length to enable the ground clearance of the model to be varied. It was not possible to obtain reliable force measurements from the balance because of the constraints created by the services exiting from the wing tips.
The angle of attack of the model was altered using two other vertical supports attached to stings downstream of its trailing edge wing tips.
The wing was unswept with a span of 2.286m (90") and had a National High Lift Programme (NHLP) section. The wing was tested in both clean and high lift configurations.
The clean wing had a chord of 0.764m (30") thus giving an aspect ratio of 3. The high lift configuration had a modified wing section with two leading edge slat surfaces (one either side of the nacelle), a trailing edge flap shroud and a single slotted full span trailing edge flap. Figure 2 shows the clean wing and propeller mounted (inverted) on the centre line of the tunnel. The high lift wing and propeller installed close to the ground can be seen in Figure 3.
The one fifth scale model propeller consisted of four carbon fibre blades with modern ARA/D sections, manufactured by Dowty Aerospace Propellers, Gloucester. The blade diameter was 0.8m (15.75") and the chord at 70% blade radius was 0.06m (2.37").
The propeller was driven by a three phase variable frequency motor of 0.14m (5.5") diameter, capable of producing 100 hp of continuous power. The motor was housed inside a representative nacelle which was faired into the spanwise centre line of the wing. The services for the motor (e.g. power supply and water cooling pipes) were passed internally along the span of the wing and exited through the wing tips.
The plane of the propeller was 0.54 blade diameters upstream of the clean wing leading edge and 0.48 blade diameters ahead of the slat leading edge when the wing was in its high lift configuration.
The nacelle and motor were aligned at 8° nose down to the wing chord line, thus reducing the propeller inflow angle as a consequence of the wing induced upwash. This angle had been predicted by use of the panel method code.
The propeller rotated clockwise when viewed from downstream of the model. The ratio of propeller disc area to tunnel cross sectional area was 0.06.
The clean and high lift wing configurations were extensively pressure tapped to enable a thorough investigation of the effect of the propeller slipstream. There were 71 chordwise tappings on the clean wing at 13 spanwise stations and a total of 121 chord wise tappings on the slat, wing and flap at the same spanwise positions. Figure 4 shows the spanwise positions of the pressure tappings on the high lift configuration. The nacelle was also extensively pressure tapped although the nacelle surface pressure distributions are not presented.

Data Acquisition and Reduction

The surface static pressures on the model were measured using a system of Scanivalve units which were situated outside of the working section. The output voltages from each pressure transducer were stored on computer and later converted to pressure coefficients based on the freestream total and static pressures.
The propeller speed was recorded using a sixty pulses per revolution tachometer attached to the motor.
The thrust and torque of the propeller were measured using a two component strain gauge balance fitted to the rear of the motor inside the nacelle.

Test Conditions

The clean and high lift wing configurations were both tested while mounted on the wind tunnel centre line. In addition, the high lift wing configuration was tested close to the ground at h/c=0.90 with the moving ground operating at the same speed as the freestream, in order to correctly simulate the effect of ground proximity. A minimum blade tip clearance of 10 cm was present when the wing was mounted at 0° angle of attack at this ground height. This gave a blade clearance to blade radius ratio of 25% which is typical of full-scale propeller aircraft. The trailing edge of the flap was situated at a distance of 0.65c above the ground plane when the propeller rotational axis was horizontal.

Under each condition, the model was tested at a range of angles of attack from -2° to 16° and at two propeller speeds of 4000 and 5000 rev/min. Measurements were also obtained with the blades removed to obtain data with the propeller slipstream absent.

The freestream velocity was maintained at 33.5 m/s (110 fps) throughout the tests, thus giving nominal propeller advance ratios of 0.503 and 0.628 and a maximum blade tip Mach number of 0.66. The thrust coefficient C_T was 0.093 and 0.127 at J=0.628 and J=0.503 respectively. The power coefficient C_P was 0.077 at J=0.628 and 0.096 at J=0.503.

The tests were performed at a blade setting angle of 20.0° measured at 70% blade radius.

The Reynolds number of the tests was 1.7×10^6 based on the chord of the clean wing. The Reynolds number of the blades at 70% radius varied between 4.8×10^5 and 5.9×10^5 for the two advance ratios.

No wind tunnel wall constraint or blockage correction factors have been included in the results. The propeller correction factor was found to be negligible.

Slipstream/Wing Interaction

The interaction between a propeller slipstream and a clean wing has been well documented in the past [1-7,10].

The slipstream has two major effects on the aerodynamic characteristics of the wing. The propeller swirl produces regions of upwash and downwash on the wing. On the upwash side, the local wing angle of attack is increased which produces an increase in the local lift coefficient. Conversely, on the downwash side the local wing angle of attack is reduced which leads to a decrease in the lift coefficient. The swirl in the slipstream therefore gives an effective twist to the wing [1,5].

The second effect is the increased dynamic head within the slipstream due to the energy added to the flow by the propeller blades. This alters the magnitude of the lift force produced on the wing washed by the slipstream but has no effect on the local lift coefficients when based on the slipstream dynamic head.

Local lift coefficients were obtained by integrating the chord wise pressure coefficients at each spanwise position and so therefore include the change in dynamic pressure.

Figure 5 shows the variation in local lift coefficient with distance from the wing centre line at 8° incidence. At J=0.628, there was a large increase in lift (compared to with the blades removed) on the area of the wing within the upwash of the slipstream. This was due to the swirl effect and increase in dynamic head combining together. At J=0.503, this effect was enhanced by the greater swirl velocity and dynamic head of the slipstream. The peak loading occurred at approximately y/R=0.50 at both advance ratios.

At J=0.628, there was a slight increase in lift on the wing within the downwash of the propeller slipstream compared to the case with the blades removed because the two slipstream effects, induced downwash and increased dynamic head, opposed each other. At J=0.503, there was a slight reduction in this loading.

The pressure distributions obtained at J=0.503 are compared to those obtained with the propeller blades removed in Figures 6 and 7 with the wing at 8° incidence. The spanwise position was y/R=0.70 either side of the wing centre line. Figure 6 shows the wing pressure distribution in the propeller downwash. The peak suction pressure coefficient was -1.6 with the propeller rotating compared to -2.2 with the blades removed and was located slightly further aft along the chord. This was a consequence of the reduced effective angle of attack. A stagnation point was present at the wing leading edge with a maximum stagnation pressure coefficient of 2.7. The wing pressure distribution in the propeller upwash can be seen in Figure 7. The peak suction pressure coefficient was -5.0 located closer to the leading edge than the corresponding pressure coefficient of -2.2 with the blades removed. The stagnation pressure coefficient of 2.7 was positioned on the wing lower surface due to the relative direction of the oncoming flow.

At 8° wing incidence and J=0.503, the stagnation pressure coefficient increased from 2.5 at y/R=0.29 to a maximum of 3.0 at y/R=0.48. The total pressure coefficient then reduced to a minimum of 2.0 within the slipstream affected part of the wing measured at y/R=0.84. This variation was due to the radial change in blade loading and resulting slipstream conditions.

The position of the stagnation point along the chord also varied within the region of the wing washed by the propeller slipstream because of the different swirl angles in the flow. At J=0.628 and y/R=0.70, the stagnation point on the upwash side of the wing moved from the leading edge to the lower surface of the wing at 3° and then moved further aft as the incidence was increased. The stagnation point on the downwash side of the wing followed the same trend but did not reach the lower surface until the wing was at 10° incidence. At J=0.503 and y/R=0.70, this effect was slightly more pronounced due to the greater swirl in the flow.

The combined effect was therefore asymmetric at both advance ratios tested. The stagnation pressure was practically the same at identical spanwise positions either side of the wing centre line but varied along the wing span with distance from the propeller rotational axis. The asymmetric effect either side of the wing centre line was only due to the rotating wake of the propeller. The change in lift coefficient when based on the local slipstream dynamic head would be equal and opposite on either side of the wing centre line. An estimate of the overall increase in lift within the slipstream was obtained by integrating the local spanwise lift coefficients. The increase in lift compared to blades off was found to be 21% and 40% for

J=0.628 and J=0.503 respectively; this net effect was due to the greater total pressure in the propeller slipstream acting on the wing. Comparable increases in lift compared to when the propeller blades were absent were obtained at each wing angle of attack studied.
Additional tests were undertaken to investigate Reynolds number effects on the propeller blades when operating at a constant advance ratio. The advance ratio was kept constant by varying both freestream velocity and propeller rotational speed. The wing pressure distribution at each spanwise position was found to be unaffected because the swirl angle in the slipstream and the increase in dynamic head of the flow were unchanged.

Slipstream/Slat/Wing/Flap Interaction

The pressure distributions based on the freestream dynamic pressure on the slat, wing and flap were integrated to calculate the lift coefficient of each component, in the same manner as for the clean wing. The slat had insufficient pressure tappings on its inner surface and so only a qualitative estimate was consequently obtained for this lifting surface.
The ratio of the local lift coefficient to the lift coefficient with the blades removed, γ, was calculated at various spanwise stations for the slat, wing and flap under different test conditions.
Figure 8 shows the variation of γ for the slat at the two advance ratios, J=0.503 and J=0.628. Clearly there were significant swirl effects on the slat. The slat pressure distribution at J=0.503 and y/R=0.70 on each side of the model at 8° is compared to the slat pressure distribution outside the slipstream in Figures 9 and 10. On the downwash side, a stagnation point occurred on the upper surface above the slat leading edge due to the relative direction of the oncoming flow. The stagnation pressure coefficient was 2.8, similar to the clean wing value under the same propeller operating conditions. This created a large flow acceleration over the slat lower surface giving rise to a large negative lift force compared to outside of the propeller slipstream. On the upwash side of the slat, the stagnation point occurred on the lower surface below the leading edge. The flow acceleration was therefore much less and a slightly greater positive lift force was created on the slat compared to outside of the slipstream. The maximum suction pressure coefficient was -6.2 on the downwash side compared to -2.5 on the upwash side and -1.3 outside of the propeller slipstream. The same trend occurred at J=0.628 but to a lesser extent.
Figures 11 and 12 show the variation of γ for the wing and flap respectively at the two advance ratios when the wing was mounted at 8° incidence. Compared to the clean wing there were very little swirl effects on the wing and flap. The slat effectively reduced the swirl in the flow before it reached the wing. The only major slipstream effect was due to the increase in total pressure of the flow. Past work with a wing and flap immersed in a propeller slipstream stated that the swirl of the flow was removed by the time it reached the flap [1]. Figures 11 and 12 do, however, show a slight increase in loading on the upwash side of the wing and flap compared to the downwash side. This suggests that although the vast majority of the swirl was removed, there was still some present in the flow.
The percentage change in lift within the slipstream affected part of the wing compared to blades off was estimated as 17% and 38% for J=0.628 and J=0.503 respectively for the model at 8° incidence. This was similar to the values calculated for the clean wing.

Effect of Ground Proximity

The ground effect tests were undertaken at a representative ground clearance for propeller aircraft. With the propeller blades removed there was an increase in lift of approximately 8% on the wing and flap at 8° wing angle of attack. This was partly due to the induced incidence caused by the ground plane which gave a slight increase in the upper surface suction peak. There was also an increase in the lower surface pressures due to the air cushion that is known to form beneath a wing in ground effect [11,12].
With the propeller blades operating, approximately the same percentage increase in lift on the wing and flap was found to occur in ground effect compared to out of ground effect, both inside and outside of the slipstream. There was no significant change in the slat pressure distribution when the model was tested close to the ground.
Figures 13 and 14 show the difference in chordwise pressure distributions for the wing and flap respectively in and out of ground effect at 8° wing incidence. The propeller was operating at J=0.503 and the spanwise position was y/R=0.70 on the upwash side of the model centre line.
These results suggest that, at this particular ground clearance, the propeller had no noticeable effect on the relative change in lift. Closer to the ground plane (limited by propeller blade clearance in this model configuration) the slipstream may be significantly deflected by the presence of the ground. This could have a marked effect on the aerodynamics of the model.

LDA Results

The results presented were obtained with the wing mounted at 8° incidence, so that the propeller axis of rotation was horizontal. The ground clearance of the model was h/c=0.90.
A set of traverses in the longitudinal direction was undertaken between the propeller disc and wing at the positions shown in Figure 15. The radial station was y/R=0.70 on the blade rising side of the model. Axial and circumferential velocities were recorded when the propeller was operating at both J=0.503 and J=0.628 and also with the blades absent. The results are shown in Tables 1 and 2.
Table 1 shows the decrease in axial velocity as the wing is approached with the propeller blades removed. The effect of increasing the propeller rotational speed can be observed by the rise in velocity. The presence of the slat created a marked reduction in velocity at traverse position D, near the leading edge of the slat. The difference between the velocities obtained for the three different test cases was also greatly reduced at this

point. The increase in axial velocity produced by increasing the propeller speed from 4000 rev/min to 5000 rev/min was similar to that seen when the blades absent and 4000 rev/min cases are compared.
The mean swirl velocities are displayed in Table 2. A small upwash velocity occurred upstream of the wing when the propeller blades were removed. An increase in upwash velocity was recorded at J=0.628 and a further increment occurred at J=0.503 although the magnitude of this change was smaller than with the axial velocity component. A significant increase in upwash velocity can be observed at traverse point D, near the slat, when the blades were rotating.
The mean velocities discussed above provide important information about the flowfield characteristics. However, in the case of rotating propellers it is also necessary to obtain data about the time dependent velocities induced by the propeller blades. An encoder was fitted to the propeller motor shaft which enabled the LDA system to record the instantaneous velocities measured over one revolution of the four blades.
The time dependent axial velocities measured at points A and D at J=0.628 are displayed in Figures 16 and 17. The passage of each blade and the resulting induced velocities can be clearly observed. The mean velocity within the slipstream decreased as the wing was approached and it can be seen that the range of instantaneous velocities followed the same trend. In addition, the increase in local axial velocity occurred over a longer time period at the position closer to the wing. The time dependent velocities measured at point A at J=0.503 can be observed in Figure 18. Although the mean slipstream axial velocity increased with propeller speed, the range of time dependent velocities was reduced.
The time dependent swirl velocities measured at points A and D are displayed in Figures 19 to 21. The variation in velocity was not as clearly defined as with the axial component and the range in time dependent velocities was generally smaller.
A similar traverse was also undertaken at a spanwise station outside of the propeller slipstream at y/R=1.33 and J=0.628. The mean velocities are displayed in Table 3. As expected there was no cyclical variation in instantaneous velocity measured at this spanwise station as displayed in Figure 22.
The LDA system was also employed to investigate the effect of the propeller slipstream at a position above the wing surface at a radial station of y/R=0.70 and 10% wing chord from the leading edge. The positions of the test points are shown in Figure 23. The variation in mean velocity with distance from the surface of the wing is shown in Table 4. The difference between the velocities measured with the blades absent and blades rotating at J=0.628 was much smaller than recorded at positions closer to the propeller disc. No large changes in unsteady velocities were recorded at position 3, as shown in Figures 24 and 25.

Theoretical Work

Panel Method

A three dimensional inviscid low order panel method was used to predict the flow around the clean and high lift wing configurations in the wind tunnel with the propeller blades removed. The panel method was based on a distribution of potential flow source panels on the surface of the configuration together with a distribution of doublet panels on the camber surface of each wing and its wake to represent lifting effects.
Neumann boundary conditions were applied at the centre point of each source panel and the set of resulting linear equations was solved for the source and doublet strengths. These strengths were then used to calculate pressure distributions over the configuration at each control point.
A relaxed wake algorithm was used whereby the wake of each lifting surface was aligned with the local freestream vector.
The theoretical code is currently under development to include a steady state surface panel method for the propeller with a semi-prescribed wake.

Results

The panel method was used to obtain theoretical data for the clean and high lift configurations in the wind tunnel with propeller blades removed. Figure 26 shows the clean wing, nacelle and spinner in the wind tunnel. Only half of the wind tunnel model is shown for convenience. Figure 27 shows the high lift wing model without the wind tunnel displayed.
Comparisons between the theoretical and experimental results at 8° angle of attack are shown in Figure 28 for the clean wing and Figures 29 to 31 for the high lift wing configuration. The results compared well considering the absence of any boundary layer or viscous effects in the code. The results also gave satisfactory agreement at the other angles of attack tested and with the high lift model in proximity to the ground.

Conclusions

On the upwash side of the clean wing, the propeller swirl and increase in dynamic head produced a large increase in wing loading. On the downwash side of the clean wing, the two effects opposed each other resulting in a comparatively small change in wing loading.
The leading edge slat significantly reduced the effect of the propeller swirl over the wing when the model was in its high lift configuration. A greater loading was produced on both sides of the wing and flap because of the increase in dynamic pressure within the propeller slipstream.
In ground effect, approximately the same percentage increase in lift was produced on the wing and flap, both inside and outside of the propeller slipstream.
The Laser Doppler Anemometer provided unsteady and time-averaged velocity data in the model flowfield.
Satisfactory results were obtained using a low order panel method for both the clean and high lift wing configurations in the wind tunnel with the propeller blades removed.

Acknowledgements

This present research was carried out under contract number

D/ERI/9/4/2040/485/XR/AERO with the Department of Trade and Industry. The authors would also like to thank British Aerospace, Woodford for their valuable assistance.

References

1. Aljabri, A.S. and Hughes, A.C. Wind tunnel investigation of the interaction of propeller slipstream with nacelle/wing/flap combinations. AGARD Conference Proceedings No. 366, Paper 21, October 1984.

2. Favier, D., Ettaouil, A., Maresca, C. and Barbi, C. Experimental and numerical study of propeller wakes in axial flight regime. Proceedings of the 16th Congress of the International Council of Aeronautical Sciences, Vol. 1, pp. 602-616, September 1988.

3. Samuelsson, I. Low speed wind tunnel investigation of propeller slipstream aerodynamic effects on different nacelle/wing combinations. Proceedings of the 16th Congress of the International Council of Aeronautical Sciences, Vol. 2, pp. 1749-1765, September 1988.

4. Witkowski, D.P., Johnston, R.T. and Sullivan, J.P. Propeller/wing interaction. AIAA Paper 89-0535.

5. Witkowski, D.P., Lee, A.K.H. and Sullivan, J.P. Aerodynamic interaction between propellers and wings. Journal of Aircraft, Vol. 26, No. 9, pp. 829-836, September 1989.

6. Samuelsson, I. Experimental investigation of low speed model propeller slipstream aerodynamic characteristics including flow field surveys and nacelle/wing static pressure measurements. Proceedings of the 17th Congress of the International Council of Aeronautical Sciences, Vol. 1, pp. 71-84, September 1990.

7. Fratello, G., Favier, D. and Maresca, C. Experimental and numerical study of the propeller/fixed wing interaction. Journal of Aircraft, Vol. 28, No. 6, pp. 365-373, June 1991.

8. Eshelby, M.E. On the aerodynamics of installed propellers. AGARD Conference Proceedings No. 366, Paper 8, October 1984.

9. Lepicovsky, J. Laser velocimeter measurements in a model propeller flowfield. Journal of Fluids Engineering, Vol. 110, pp. 350-354, December 1988.

10. Johnston, R.T., Witkowski, D.P. and Sullivan, J.P. Propeller wakes and their interaction with wings. Proceedings of the 9th International Symposium on Air Breathing Engines, Vol. 2, pp. 1070-1077, September 1989.

11. Tani, I., Taima, M. and Simidu, S. The effect of ground on the aerodynamic characteristics of a monoplane wing. Report No. 156, Vol. XIII, Aeronautical Research Institute, Tokyo Imperial University, September 1937.

12. Serebrisky, Y.M. and Biachuev, S.A. Wind-tunnel investigation of the horizontal motion of a wing near the ground. NACA Technical Memorandum No. 1095, September 1946.

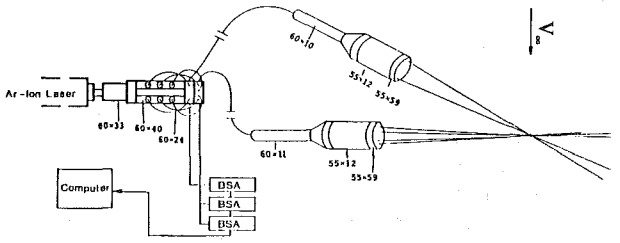

Figure 1. Laser Doppler Anemometer system.

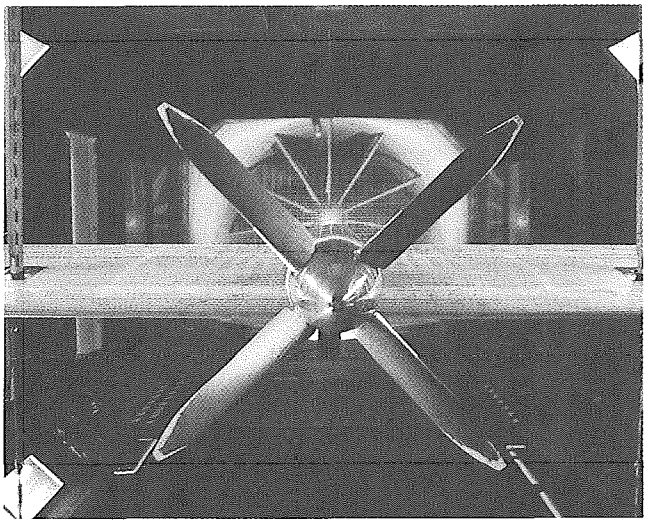

Figure 2. Clean wing and propeller mounted out of ground effect.

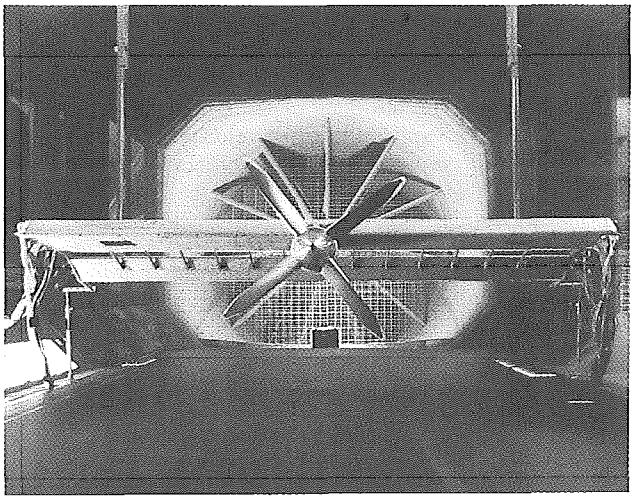

Figure 3. High lift wing and propeller mounted in ground effect.

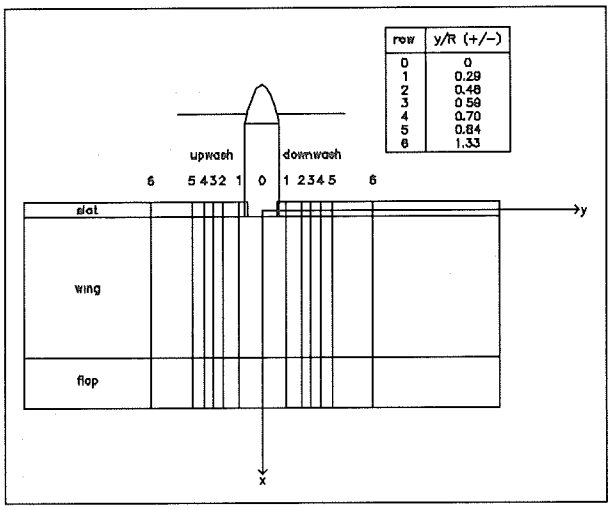

Figure 4. Spanwise positions of the pressure tappings on the high lift wing.

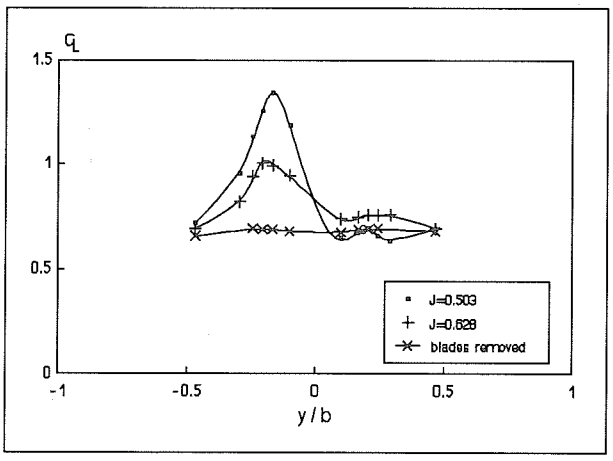

Figure 5. Clean wing loading.

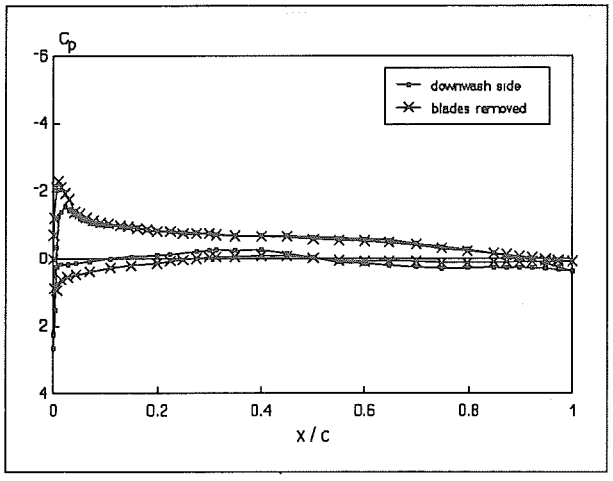

Figure 6. Clean wing pressure distribution in propeller downwash.

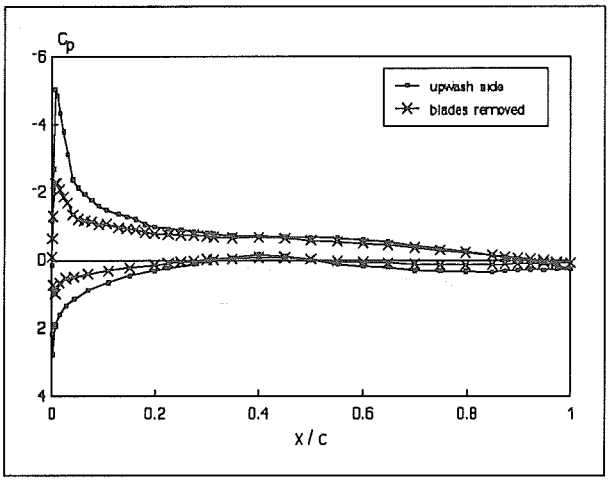

Figure 7. Clean wing pressure distribution in propeller upwash.

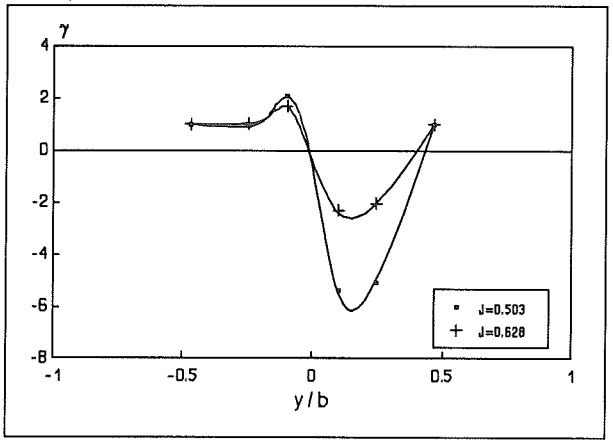

Figure 8. Change in slat loading.

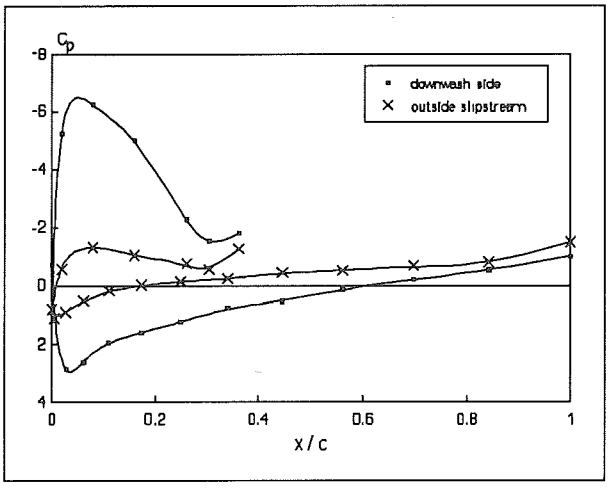

Figure 9. Slat pressure distribution in propeller downwash.

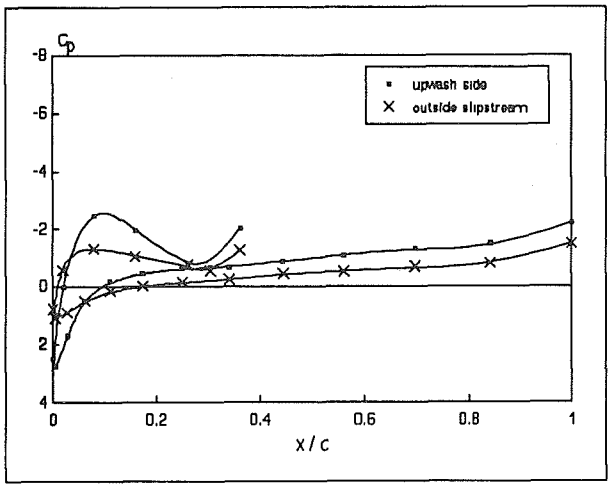

Figure 10. Slat pressure distribution in propeller upwash.

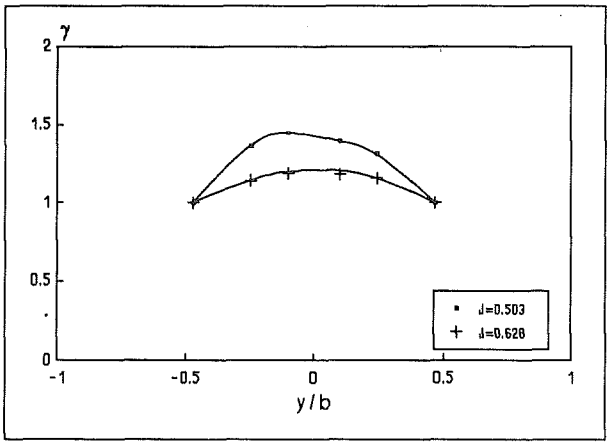

Figure 11. Change in wing loading.

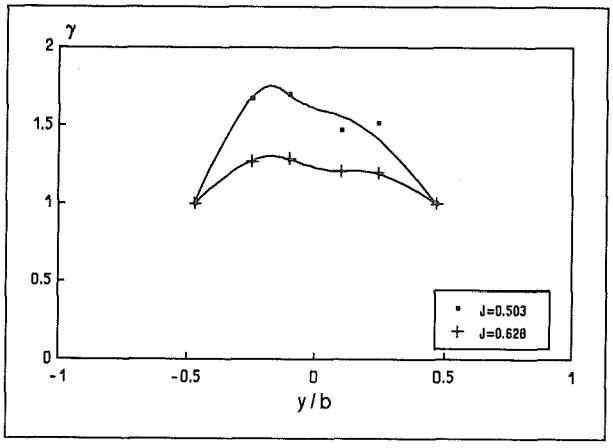

Figure 12. Change in flap loading.

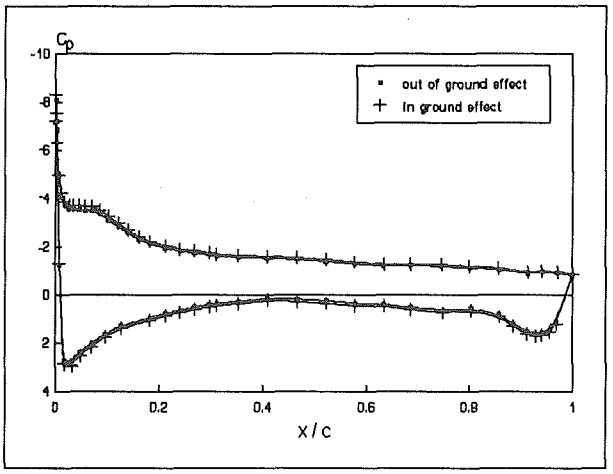

Figure 13. Wing pressure distribution in and out of ground effect.

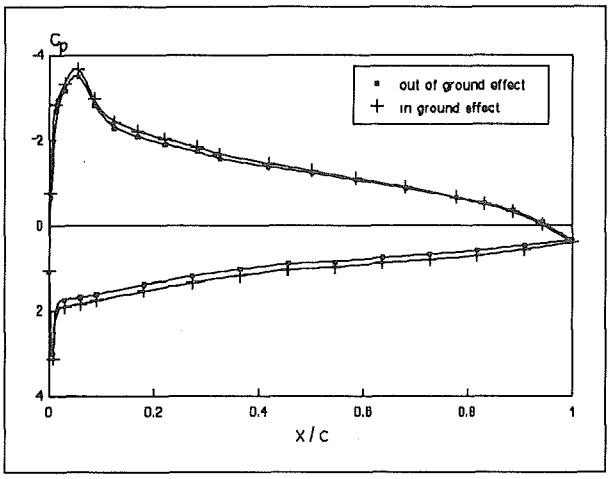

Figure 14. Flap pressure distribution in and out of ground effect.

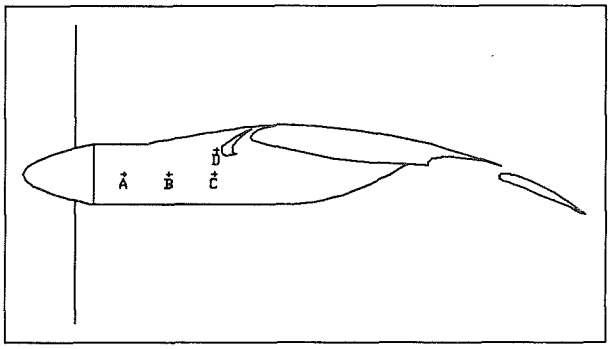

Figure 15. Longitudinal traverse positions between propeller and wing.

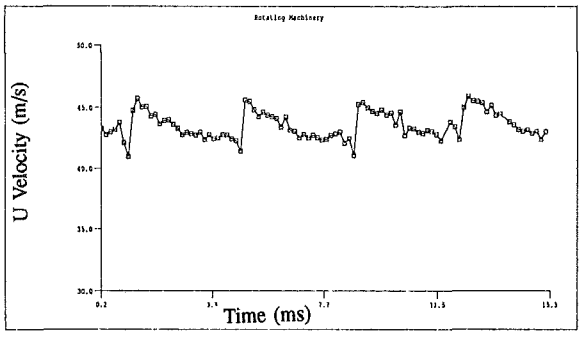

Figure 16. Unsteady slipstream axial velocity, y/R=0.70, position A, J=0.628.

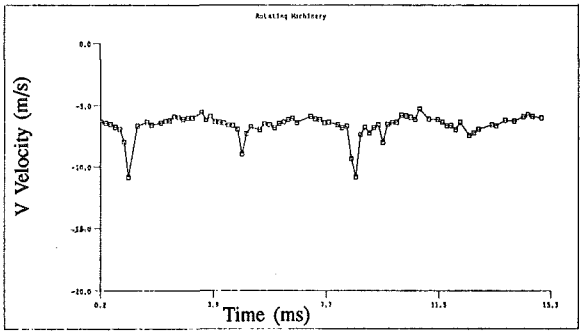

Figure 19. Unsteady slipstream swirl velocity, y/R=0.70, position A, J=0.628.

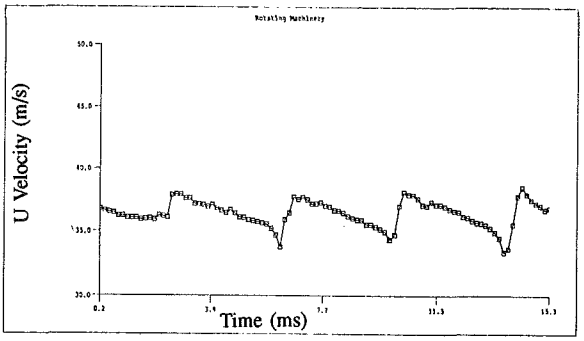

Figure 17. Unsteady slipstream axial velocity, y/R=0.70, position D, J=0.628.

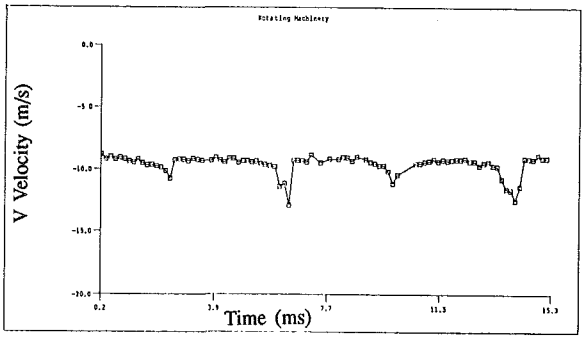

Figure 20. Unsteady slipstream swirl velocity, y/R=0.70, position D, J=0.628.

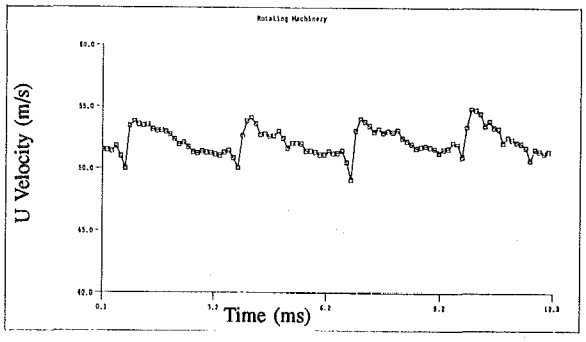

Figure 18. Unsteady slipstream axial velocity, y/R=0.70, position A, J=0.503.

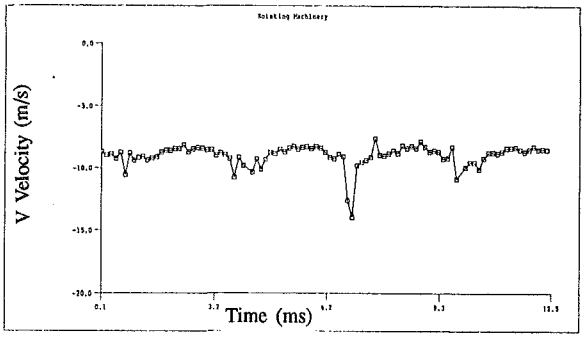

Figure 21. Unsteady slipstream swirl velocity, y/R=0.70, position A, J=0.503.

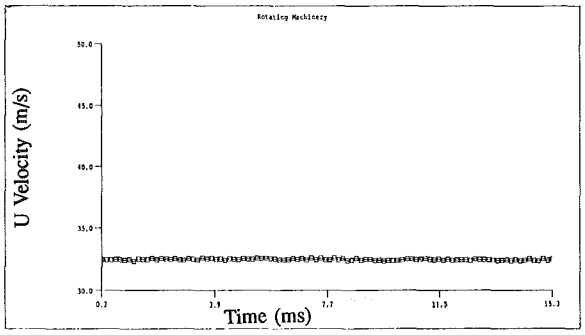

Figure 22. Unsteady slipstream axial velocity, y/R=1.33, position A, J=0.628.

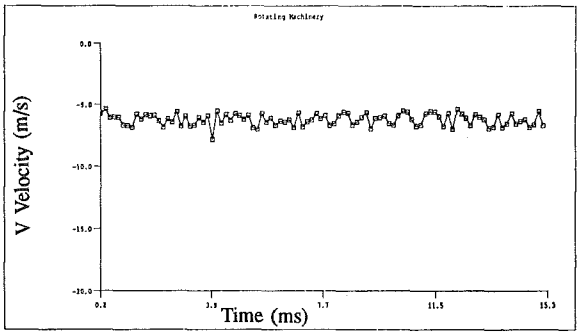

Figure 25. Unsteady vertical velocity at position 3 over wing, blades removed.

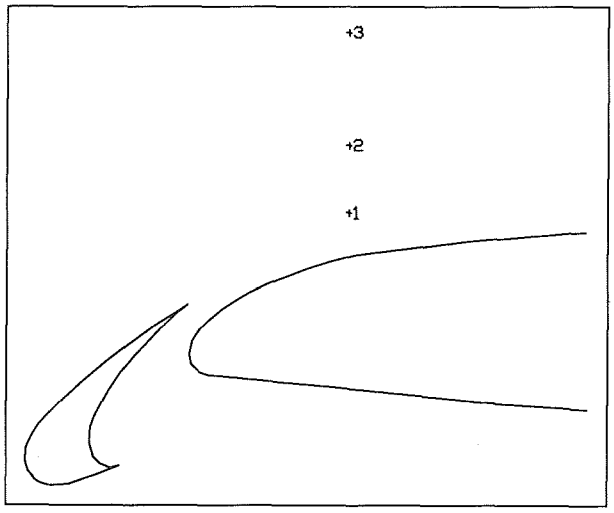

Figure 23. Traverse positions over wing.

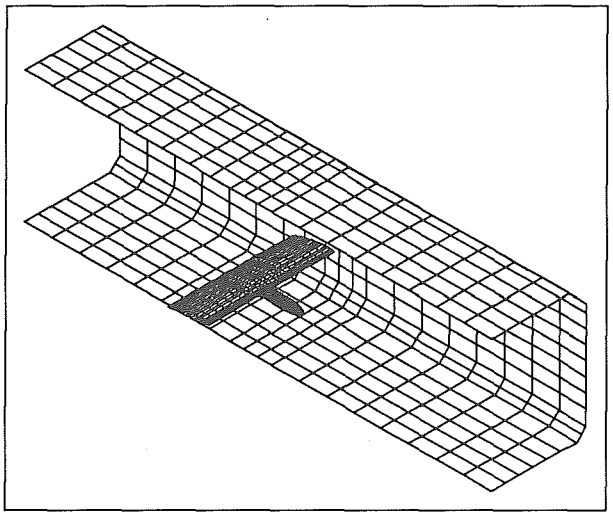

Figure 26. Clean wing and wind tunnel panel geometry.

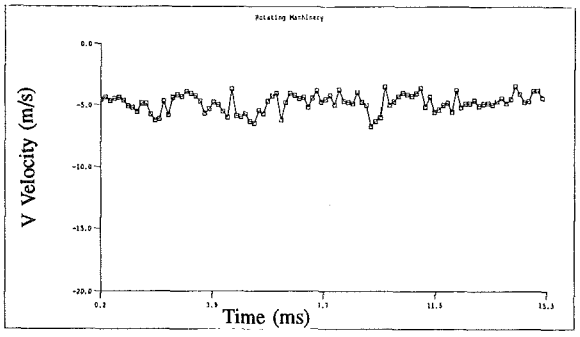

Figure 24. Unsteady vertical velocity at position 3 over wing, J=0.628.

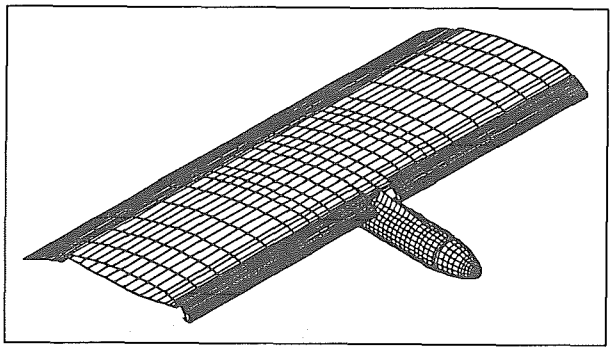

Figure 27. High lift wing panel geometry.

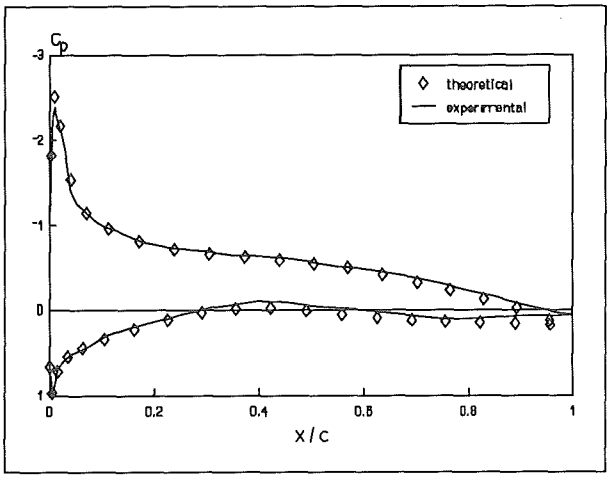

Figure 28. Clean wing pressure distributions

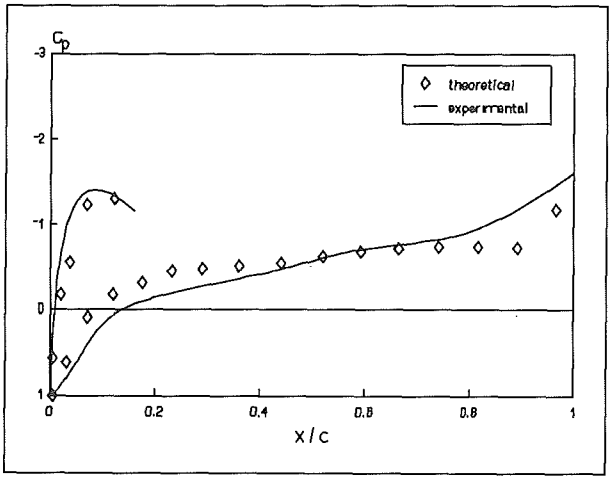

Figure 29. Slat pressure distributions.

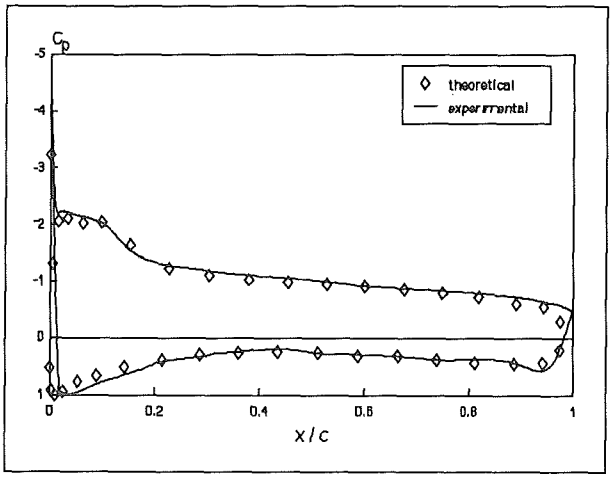

Figure 30. Wing pressure distributions.

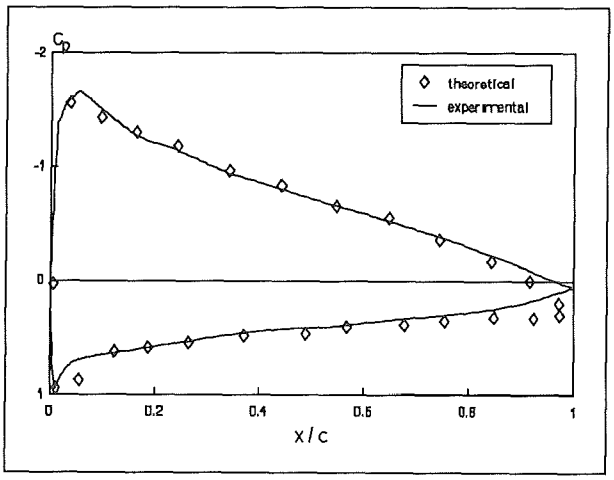

Figure 31. Flap pressure distributions.

Position	d (mm)	J=0.628	J=0.503	Blades removed
A	130	43.63	52.16	-
B	250	42.94	51.94	32.10
C	370	41.96	51.51	30.50
D	375	36.17	43.55	30.39

Table 1. Mean axial slipstream velocities between propeller and wing, y/R=0.70.

Position	d (mm)	J=0.628	J=0.503	Blades removed
A	130	6.66	8.87	2.50
B	250	-	9.96	3.22
C	370	6.46	7.11	2.49
D	375	9.73	10.55	2.66

Table 2. Mean swirl slipstream velocities between propeller and wing, y/R=0.70.

Position	d (mm)	U_{MEAN} ($m.s^{-1}$)	V_{MEAN} ($m.s^{-1}$)
A	130	32.45	2.46
B	250	30.86	3.27
C	370	29.50	2.58
D	375	25.21	5.66

Table 3. Mean axial and swirl velocities, y/R=1.33.

Position number	U_{MEAN} ($m.s^{-1}$)		V_{MEAN} ($m.s^{-1}$)	
	J=0.628	Blades removed	J=0.628	Blades removed
1	52.80	55.98	5.84	-
2	54.07	52.28	6.72	7.43
3	48.87	48.26	4.78	6.22

Table 4. Mean velocities above wing surface.